JOURNAL OF COMPUTATIONAL PHYSICS **133,** 6–17 (1997)
ARTICLE NO. CP965584

Quasi-ENO Schemes for Unstructured Meshes Based on Unlimited Data-Dependent Least-Squares Reconstruction

Carl F. Ollivier-Gooch

Mathematics and Computer Science Division, Argonne National Laboratory, Argonne, Illinois 60439
E-mail: gooch@mcs.anl.gov

Received December 26, 1995; revised September 4, 1996

A crucial step in obtaining high-order accurate steady-state solutions to the Euler and Navier–Stokes equations is the high-order accurate reconstruction of the solution from cell-averaged values. Only after this reconstruction has been completed can the flux integral around a control volume be accurately assessed. In this work, a new reconstruction scheme is presented that is conservative, is uniformly accurate, allows only asymptotically small overshoots, is easy to implement on arbitrary meshes, has good convergence properties, and is computationally efficient. The new scheme, called DD-L_2-ENO, uses a data-dependent weighted least-squares reconstruction with a fixed stencil. The weights are chosen to strongly emphasize smooth data in the reconstruction, satisfying the weighted ENO conditions of Liu, Osher, and Chan. Because DD-L_2-ENO is designed in the framework of k-exact reconstruction, existing techniques for implementing such reconstructions on arbitrary meshes can be used. The scheme allows graceful degradation of accuracy in regions where insufficient smooth data exists for reconstruction of the requested high order. Similarities with and differences from WENO schemes are highlighted. The asymptotic behavior of the scheme in reconstructing smooth and piecewise smooth functions is demonstrated. DD-L_2-ENO produces uniformly high-order accurate reconstructions, even in the presence of discontinuities. Results are shown for one-dimensional scalar propagation and shock tube problems. Encouraging preliminary two-dimensional flow solutions obtained using DD-L_2-ENO reconstruction are also shown and compared with solutions using limited least-squares reconstruction.

1. INTRODUCTION

A crucial step in obtaining high-order accurate steady-state solutions to the Euler and Navier–Stokes equations is the high-order accurate reconstruction of the solution from cell-averaged values. Only after this reconstruction has been completed can the flux integral around a control volume be accurately assessed. Ideally, the reconstruction should conserve the mean value of the function in each cell, be uniformly accurate with no overshoots, have good steady-state convergence properties, be computationally efficient and be easy to implement on arbitrary meshes. In particular, the scheme must be easy to implement on meshes for which the local mesh connectivity is variable. The variable connectivity, not the shape of the cells, is the key distinguishing feature of unstructured versus structured meshes in a reconstruction context.

Both limited k-exact reconstruction and essentially non-oscillatory (ENO) reconstruction have many of these desirable properties. The design criteria for k-exact reconstruction given by Barth and Frederickson [1] ensure conservation of the mean, good accuracy for smooth functions, and computational efficiency. These schemes are easy to implement on arbitrary meshes. A fixed stencil is used, allowing precomputation of certain purely geometric quantities used in the reconstruction, with a corresponding improvement in efficiency. Accuracy near discontinuities is poor, however, and limiting is required to prevent overshoots of $O(1)$. Limiters that retain good convergence properties (e.g., [2]) are often computationally expensive.

By design, the ENO reconstruction schemes of Harten *et al.* [3–5] conserve the mean, are uniformly accurate at all points for which a smooth neighborhood exists, and guarantee that overshoots will be no larger than the order of the truncation error of the reconstruction. Uniform high-order accuracy is obtained by using reconstruction stencils that vary in both space and time. Unfortunately, such stencils can hamper convergence to steady state. The weighted ENO (WENO) family of schemes overcomes this difficulty by using all possible stencils with a data-dependent weighting [6, 7]. Stencils containing nonsmooth data are not excluded by these schemes, but instead are given a weight on the order of the truncation error. Because the weights vary smoothly with the data, these schemes converge well. With proper choice of weights, WENO schemes can attain $(2k + 1)$-order accuracy for smooth functions using $(k + 1)$-point stencils [7]. These schemes are one-dimensional in nature and are applied direction-by-direction for reconstruction on multidimensional structured meshes.

The implementation of stencil-searching ENO schemes on unstructured meshes is difficult because stencils must be sought for all dimensions simultaneously and because

0021-9991/97 $25.00

the number of possible stencils is very large [8, 9]. The WENO family holds out some promise here, in that each of a set of stencils could be included with a data-dependent weight, eliminating the need for complex logic to find a smooth stencil. Nevertheless, such schemes would still be hampered in practice because there may be no smooth stencil; graceful recovery in this situation is not a subject discussed in the literature.

In this work, a new reconstruction scheme is presented that has the best properties of both limited k-exact reconstruction schemes and ENO schemes. The new scheme, called DD-L_2-ENO, uses a data-dependent weighted least-squares reconstruction with a fixed stencil. To this extent, the scheme resembles existing k-exact reconstruction algorithms [1, 10] and can build on that technology base. The feature which distinguishes DD-L_2-ENO from standard k-exact schemes is the use of *data-dependent* weights. Each point in a reconstruction stencil is given a data-dependent weight, chosen to strongly emphasize smooth data in the reconstruction. Specifically, the weight given to nonsmooth data is on the order of the truncation error. In this respect, DD-L_2-ENO is similar to WENO schemes, except that the point-wise nature of the weighting with DD-L_2-ENO imparts some additional flexibility in choosing the smooth data to include in the reconstruction. For both DD-L_2-ENO and WENO schemes, the weights vary smoothly with variations in the data, which improves steady-state convergence in comparison to stencil-searching ENO schemes. In regions where insufficient smooth data is available for high-order reconstruction, DD-L_2-ENO automatically reduces the order of accuracy of the reconstruction locally; this should improve robustness in practice.

Section 2 reviews WENO reconstruction schemes in one dimension. Section 3 presents the new data-dependent least-squares reconstruction, including discussion of the computation of the data-dependent weights and requirements for the algorithm used to solve the least-squares problem. Section 4 shows results for reconstruction of smooth and nonsmooth functions, including solutions to the scalar wave equation. In Section 5, some sample flow solutions are shown.

2. WEIGHTED ENO RECONSTRUCTION

The criteria set forth by Harten *et al.* [5] for essentially nonoscillatory reconstruction place a great emphasis on accuracy, in that ENO schemes obtain high-order accurate reconstructions for all control volumes having a smooth neighborhood. Also, ENO reconstruction conserves the mean and, in one dimension, guarantees that the total variation of the reconstruction will not exceed that of the original function by more than $O(\Delta x^{k+1})$.

The weighted ENO (WENO) schemes of Liu, Osher, and Chan [6] take a somewhat different approach to nonsmooth data. ENO schemes try to find the smoothest possible stencil of $k + 1$ points containing the control volume in question; $k + 1$ stencils exist. WENO schemes use a convex combination of reconstructions using each possible stencil, with weights that can be written as

$$w_i = \frac{\alpha_i}{\sum_{i=0}^{k} \alpha_i}. \tag{1}$$

When the function is smooth, each stencil provides a $(k + 1)$-order accurate reconstruction. In this case, the α_i can be chosen to give $(2k + 1)$-order accuracy [7]. On the other hand, when the data in a stencil is nonsmooth, the weight for that stencil is on the order of the truncation error. Liu, Osher, and Chan [6] define this as the "ENO property" for WENO schemes. For a more complete discussion of these schemes, see [6, 7].

3. DATA-DEPENDENT LEAST-SQUARES ENO RECONSTRUCTION

Rather than beginning with a direction-by-direction ENO scheme and adapting it to unstructured meshes, we take the opposite approach: begin with a least-squares reconstruction scheme suitable for use on unstructured meshes and modify it to satisfy the ENO property. That is, we seek to solve the following problem:

Consider a domain Ω which has been tessellated; the tessellation has a characteristic length scale Δx, at least locally. The median dual of the tessellation defines for each vertex v_i a surrounding control volume V_i. For any function $u(\mathbf{x})$ defined on Ω and its control-volume averaged values $\overline{u}_i$, compute an expansion $R_i(\mathbf{x} - \mathbf{x}_i)$ about v_i that

- conserves the mean
- has compact support
- reconstructs exactly polynomials of degree $\leq k$. Equivalently, $R_i(\mathbf{x} - \mathbf{x}_i) - u(\mathbf{x}) = O(\Delta x^{k+1})$
- satisfies the ENO property of Liu, Osher, and Chan [6].

The remainder of this section will describe this process in two dimensions. Reduction to one dimension, extension to three dimensions, and application to structured meshes are all straightforward variations on the theme.

3.1. *Conservation of the Mean*

Conservation of the mean within a control volume requires that

$$\int_{V_i} R_i(\mathbf{x} - \mathbf{x}_i)\, dA = \int_{V_i} u(\mathbf{x})\, dA. \tag{2}$$

This can be accomplished by using zero-mean polynomials in expanding about v_i. That is, by writing

$$
\begin{aligned}
R_i(\mathbf{x}-\mathbf{x}_i) = \overline{u}_i &+ \left.\frac{\partial u}{\partial x}\right|_i (x - x_i - \overline{x}_i) \\
&+ \left.\frac{\partial u}{\partial y}\right|_i (y - y_i - \overline{y}_i) \\
&+ \left.\frac{\partial^2 u}{\partial x^2}\right|_i \frac{(x-x_i)^2 - \overline{x_i^2}}{2} \\
&+ \left.\frac{\partial^2 u}{\partial x\,\partial y}\right|_i ((x-x_i)(y-y_i) - \overline{xy}_i) \\
&+ \left.\frac{\partial^2 u}{\partial y^2}\right|_i \frac{(y-y_i)^2 - \overline{y_i^2}}{2} + \cdots,
\end{aligned} \tag{3}
$$

where

$$
\overline{x^n y^m} \equiv \frac{1}{A_i}\int_{V_i} (x-x_i)^n (y-y_i)^m \, dA. \tag{4}
$$

By inspection, the expansion of Eq. (3) satisfies Eq. (2). As a practical matter, the integral of Eq. (4) is most easily computed by using Green's theorem to convert it to a boundary integral around V_i,

$$
\overline{x^n y^m} = \frac{1}{(n+1)A_i}\int_{\partial V_i} (x-x_i)^{n+1}(y-y_i)^m \, dy. \tag{5}
$$

This integral may be evaluated exactly using a Gaussian quadrature of appropriate order along the boundary of the control volume.

3.2. *Compact Support*

Compact support implies that the reconstruction R_i will not require data that is too far removed physically from $\mathbf{x}_i$. This in turn implies, for reasonable meshes, that data used in R_i will not be topologically far from control volume i; that is, there will be a small number of levels of neighbors used to compute R_i. Conversely, using only a small topological neighborhood of a vertex in the reconstruction ensures compact physical support as well. For first- and second-order accuracy ($k = 0, 1$) in two dimensions, control volumes adjacent to V_i (the first neighbors) are used to form the set $\{V_j\}_i$ of control volumes in the reconstruction stencil. For third- and fourth-order accuracy ($k = 2, 3$), second neighbors are also included in $\{V_j\}_i$. Because stencil determination is done as a preprocessing step, it is possible to add members to the stencils of control volumes which are too near the boundary to have sufficient support for the desired order of accuracy of reconstruction.

3.3. *Accuracy for Smooth Functions*

Accuracy of the reconstruction for smooth functions can be stated in two equivalent ways. The reconstruction can be said to be k-exact for some k if, when reconstructing $P(\mathbf{x}) \in \{x^m y^n : m + n \le k\}$,

$$
R_i(\mathbf{x}-\mathbf{x}_i) \equiv P(\mathbf{x}). \tag{6}
$$

Alternatively, one can say that for any $u(\mathbf{x})$,

$$
R_i(\mathbf{x}-\mathbf{x}_i) = u(\mathbf{x}) + O(\Delta x^{k+1}). \tag{7}
$$

In practice, this accuracy requirement means that the modified Taylor series expansion of R_i given in Eq. (3) must be carried out through the k^{th} derivatives. To compute these derivatives, we seek to minimize the error in predicting the mean value of the function for control volumes in the stencil $\{V_j\}_i$. The mean value, for a single control volume V_j, of the reconstructed function R_i is

$$
\begin{aligned}
&\frac{1}{A_j}\int_{V_j} R_i(\mathbf{x}-\mathbf{x}_i)\, dA \\
&\quad = \overline{u}_i + \left.\frac{\partial u}{\partial x}\right|_i \left(\frac{1}{A_j}\int_{V_j} (x-x_i)\, dA - \overline{x}_i\right) \\
&\qquad + \left.\frac{\partial u}{\partial y}\right|_i \left(\frac{1}{A_j}\int_{V_j} (y-y_i)\, dA - \overline{x}_i\right) \\
&\qquad + \left.\frac{\partial^2 u}{\partial x^2}\right|_i \left(\frac{1}{2A_j}\int_{V_j} (x-x_i)^2\, dA - \frac{1}{2}\overline{x_i^2}\right) \\
&\qquad + \left.\frac{\partial^2 u}{\partial x\,\partial y}\right|_i \left(\frac{1}{A_j}\int_{V_j} (x-x_i)(y-y_i)\, dA - \overline{xy}_i\right) \\
&\qquad + \left.\frac{\partial^2 u}{\partial y^2}\right|_i \left(\frac{1}{2A_j}\int_{V_j} (y-y_i)^2\, dA - \frac{1}{2}\overline{y_i^2}\right) + \cdots.
\end{aligned} \tag{8}
$$

To avoid computing moments of each control volume in $\{V_j\}_i$ about v_i, replace $x - x_i$ and $y - y_i$ with $(x - x_j) + (x_j - x_i)$ and $(y - y_j) + (y_j - y_i)$, respectively. Expanding and integrating,

$$
\begin{aligned}
&\frac{1}{A_j}\int_{V_j} R_i(\mathbf{x}-\mathbf{x}_i) \\
&\quad = \overline{u}_i + \left.\frac{\partial u}{\partial x}\right|_i (\overline{x}_j + (x_j - x_i) - \overline{x}_i) \\
&\qquad + \left.\frac{\partial u}{\partial y}\right|_i (\overline{y}_j + (y_j - y_i) - \overline{y}_i) \\
&\qquad + \left.\frac{\partial^2 u}{\partial x^2}\right|_i \frac{\overline{x_j^2} + 2\overline{x}_j(x_j - x_i) + (x_j - x_i)^2 - \overline{x_i^2}}{2} \\
&\qquad + \left.\frac{\partial^2 u}{\partial x\,\partial y}\right|_i (\overline{xy}_j + \overline{x}_j(y_j - y_i) + (x_j - x_i)\overline{y}_j \\
&\qquad + (x_j - x_i)(y_j - y_i) - \overline{xy}_i) \\
&\qquad + \left.\frac{\partial^2 u}{\partial y^2}\right|_i \frac{\overline{y_j^2} + 2\overline{y}_j(y_j - y_i) + (y_j - y_i)^2 - \overline{y_i^2}}{2} + \cdots.
\end{aligned} \tag{9}
$$

The geometric terms in this equation are of the general form

$$\begin{aligned}\widehat{x^n y_{ij}^m} &\equiv \frac{1}{A_j}\int_{V_j}((x-x_j)+(x_j-x_i))^n \\ &\quad\times((y-y_j)+(y_j-y_i))^m\,dA - \overline{x^n y_i^m} \\ &= \sum_{l=0}^{m}\sum_{k=0}^{n}\binom{m}{l}\binom{n}{k}(x_j-x_i)^k \\ &\quad\times(y_j-y_i)^l\overline{x^{n-k}y_j^{m-l}} - \overline{x^n y_i^m}.\end{aligned} \tag{10}$$

In these terms, we can write

$$\begin{aligned}\frac{1}{A_j}\int_{V_j}R_i(\mathbf{x}-\mathbf{x}_i) = \overline{u}_i &+ \left.\frac{\partial u}{\partial x}\right|_i \hat{x}_{ij} + \left.\frac{\partial u}{\partial y}\right|_i \hat{y}_{ij} + \left.\frac{\partial^2 u}{\partial x^2}\right|_i \frac{\widehat{x_{ij}^2}}{2} \\ &+ \left.\frac{\partial^2 u}{\partial x\,\partial y}\right|_i \widehat{xy}_{ij} + \left.\frac{\partial^2 u}{\partial y^2}\right|_i \frac{\widehat{y_{ij}^2}}{2} + \cdots.\end{aligned} \tag{11}$$

Equation (11) evaluates the mean value of the reconstruction $R_i(\mathbf{x}-\mathbf{x}_i)$ for a control volume j, given the low-order derivatives of the solution at v_i and low-order moments of the control volumes. The difference between this prediction and the actual control-volume average $\overline{u}_j$ is easy to assess. The derivatives at v_i are chosen to minimize this error over the stencil $\{V_j\}_i$ in a least-squares sense. Geometric weights w_{ij} are used to specify the relative importance of good prediction for various control volumes in the stencil, with the weights based on distance between vertices. The resulting least-squares problem is

$$\begin{bmatrix} L_{i1} \\ L_{i2} \\ L_{i3} \\ \vdots \\ L_{iN} \end{bmatrix} \begin{pmatrix} \dfrac{\partial u}{\partial x} \\ \dfrac{\partial u}{\partial y} \\ \dfrac{1}{2}\dfrac{\partial^2 u}{\partial x^2} \\ \dfrac{\partial^2 u}{\partial x \partial y} \\ \dfrac{1}{2}\dfrac{\partial^2 u}{\partial y^2} \\ \vdots \end{pmatrix}_i = \begin{pmatrix} w_{i1}(\overline{u}_1 - \overline{u}_i) \\ w_{i2}(\overline{u}_2 - \overline{u}_i) \\ w_{i3}(\overline{u}_3 - \overline{u}_i) \\ \vdots \\ w_{iN}(\overline{u}_N - \overline{u}_i) \end{pmatrix}, \tag{12}$$

where

$$L_{ij} = (w_{ij}\hat{x}_{ij}\, w_{ij}\hat{y}_{ij}\, w_{ij}\widehat{x_{ij}^2}\, w_{ij}\widehat{xy}_{ij}\, w_{ij}\widehat{y_{ij}^2}\cdots) \tag{13}$$

and

$$w_{ij} = \frac{1}{|\mathbf{x}_j - \mathbf{x}_i|^2}. \tag{14}$$

The least-squares problem of Eq. (12) is solved using Householder transformations to reduce the left-hand side of Eq. (12) to upper-triangular form. After the upper-triangularization is complete, back-substitution yields the required derivatives. There are several good reasons to use this approach instead of the simpler normal equation solution to the least-squares problem:

- Using Householder transformations gives a more accurate solution to the least-squares problem than using normal equations, especially for ill-conditioned matrices. The error in the solution is $O(\varepsilon K)$ using Householder transformations and $O(\varepsilon K^2)$ for normal equations, where K is the condition number of the nonsquare matrix and ε is machine precision [11]. This also implies greater robustness.
- As a further improvement in robustness, the Householder transform approach can detect singular and nearly singular matrices on the fly. If the least-squares problem is (nearly) singular, a column with (nearly) zero elements on the below the diagonal will be encountered during Householder triangularization. This failure occurs because the stencil is inadequate to support the requested number of derivatives. To resolve this, either more points must be added to the reconstruction stencil or the reconstruction must be modified to include fewer derivatives. The latter course is adopted in this work. Derivatives are computed only to the highest order for which *all* derivatives can be computed; the additional incomplete set of derivatives is discarded, because no increase in order of accuracy is possible by retaining them.
- After the upper-triangularization of the least-squares problem is complete, the residual for the solution is available at virtually no cost. Before back-substitution, the problem looks like:

$$\begin{bmatrix} x & x & x & \cdots & x \\ & x & x & \cdots & x \\ & & x & \cdots & x \\ & & & \ddots & x \\ & & & & x \\ & & 0 & & \\ & & m\times n & & \end{bmatrix} \begin{pmatrix} \dfrac{\partial u}{\partial x} \\ \dfrac{\partial u}{\partial y} \\ \dfrac{1}{2}\dfrac{\partial^2 u}{\partial x^2} \\ \dfrac{\partial^2 u}{\partial x \partial y} \\ \dfrac{1}{2}\dfrac{\partial^2 u}{\partial y^2} \\ \vdots \end{pmatrix}_i = \begin{pmatrix} r_1 \\ r_2 \\ \vdots \\ r_m \\ r_{m+1} \\ \vdots \\ r_{n-1} \\ r_n \end{pmatrix}. \tag{15}$$

Clearly, the first m equations will be satisfied exactly. The

remaining $n - m$ equations will not be; the residual $\mathscr{R}$, which is the same as the residual for the original problem, is

$$\mathscr{R} = \sqrt{\sum_{l=m+1}^{n} r_l^2}. \tag{16}$$

This residual will be put to use in computing data-dependent weights to enforce the ENO property, after scaling by Δx^2 to remove the effects of the geometric weighting term.

3.4. *ENO Property*

The reconstruction scheme described above is designed for smooth functions. For nonsmooth functions—those with $O(1)$ discontinuities—such a scheme allows overshoots of $O(1)$. This is not desirable for either function approximation or scientific computation, where such overshoots can easily produce aphysical values. This problem has typically been addressed by performing a reconstruction with geometric weights and preventing overshoots by heuristically *limiting*, or reducing, the derivatives (e.g., [10, 2]). While this approach is not unsuccessful, it provides only a mechanical solution to an underlying theoretical problem. Specifically, the stencil for a control volume i near a discontinuity will include control volumes j which lie across the discontinuity. Because the function is not smooth, approximating data in V_j by a modified Taylor series around v_i is inappropriate. Ignoring this mathematical fact causes the unphysically large derivatives that limiting seeks to reduce.

A better alternative is to reconstruct using only data that *is* smoothly connected to data in i. This approach is taken directly by typical ENO schemes, which by design search for a smooth stencil and completely exclude nonsmooth data from the reconstruction. WENO schemes work less directly, weighting all possible stencils and weighting those containing nonsmooth data with a weight that is of the order of the truncation error.

In a weighted least-squares context, weights are assigned to control volumes rather than to stencils. Nevertheless, the goal is to weight nonsmooth data with $O(\Delta x^{k+1})$ to satisfy the ENO condition of Liu, Osher, and Chan [6]. We seek to construct a data-dependent weight, which will multiply the previously calculated geometric weight. This construction is based on two observations:

1. If the function is nonsmooth, and if the neighborhood of V_i crosses a discontinuity, then a modified Taylor expansion does not adequately describe the function locally and there will be one or more control volumes j for which

$$\frac{1}{A_j}\int_{V_j} R_i(\mathbf{x} - \mathbf{x}_i)\, dA - \overline{u}_j = O(1). \tag{17}$$

This means that the residual $\mathscr{R}$ of the least-squares problem will be $O(1)$. On the other hand, for stencils which cover only smooth regions of the function,

$$R_i(\mathbf{x} - \mathbf{x}_i) - u(\mathbf{x}) = O(\Delta x^{k+1}) \tag{18}$$

and $\mathscr{R}$ is also $O(\Delta x^{k+1})$. Therefore, $\mathscr{R}$ can be used as a guage of the smoothness of the data for the entire stencil $\{V_j\}_i$.

2. Whether the data in V_j is smoothly connected to data in V_i can be determined asymptotically by evaluating

$$\frac{u_j - u_i}{|\mathbf{x}_j - \mathbf{x}_i|} = \begin{cases} O(1), & \text{smoothly connected;} \\ O(\Delta x^{-1}), & \text{not smoothly connected.} \end{cases} \tag{19}$$

We seek a data-dependent weighting which uses $\mathscr{R}$ to detect stencils with nonsmooth data and $(u_j - u_i)/|\mathbf{x}_j - \mathbf{x}_i|$ to determine which data within that stencil should be excluded and which included. Put another way, we seek to construct a *smoothness indicator* analogous to the divided difference indicators of [6, 7] which is appropriate for unstructured meshes and least-squares reconstruction. One appropriate weighting is

$$W_{ij}^{\mathrm{DD}} = 1 \Big/ \left(\varepsilon + \mathscr{R} l^2 \left| \frac{u_j - u_i}{|\mathbf{x}_j - \mathbf{x}_i|} \right|^{(k+1)} \right), \tag{20}$$

where $\varepsilon = 10^{-10}$ prevents division by zero; l, a length scale for the control volume i, is included to remove the effects of the geometric weighting on $\mathscr{R}$; $\mathscr{R} l^2 |(u_j - u_i)/|\mathbf{x}_j - \mathbf{x}_i||^{(k+1)}$ is the smoothness indicator.

Asymptotically, the behavior of this weighting for the three important cases is

$$W_{ij}^{\mathrm{DD}} = \begin{cases} \max(\varepsilon^{-1}, O(\Delta x^{-(k+1)})), & \text{smooth function,} \\ O(1) & \text{smooth data in stencil with non-smooth data,} \\ O(\Delta x^{(k+1)}), & \text{non-smooth data.} \end{cases} \tag{21}$$

In summary, for stencils containing only smoothly connected data, the data-dependent weights are all of same order, ensuring that the good qualities of the data-independent reconstruction will be preserved for smooth functions. For stencils that are not entirely smooth, the data-dependent weight for nonsmooth data is smaller than that for smooth data by a factor of the order of truncation error. These weightings satisfy the ENO condition of Liu, Osher, and Chan [6].

Once the data-dependent weight has been computed for each control volume j in the stencil, the j^{th} row in the least-squares problem is scaled by it. Without any computation

other than this scaling, the least-squares problem of Eq. (12) can be modified to

$$\begin{bmatrix} L'_{i1} \\ L'_{i2} \\ L'_{i3} \\ \vdots \\ L'_{iN} \end{bmatrix} \begin{pmatrix} \dfrac{\partial u}{\partial x} \\ \dfrac{\partial u}{\partial y} \\ \dfrac{1}{2}\dfrac{\partial^2 u}{\partial x^2} \\ \dfrac{\partial^2 u}{\partial x \partial y} \\ \dfrac{1}{2}\dfrac{\partial^2 u}{\partial y^2} \\ \vdots \end{pmatrix}_i = \begin{pmatrix} w'_{i1}(\overline{u}_1 - \overline{u}_i) \\ w'_{i2}(\overline{u}_2 - \overline{u}_i) \\ w'_{i3}(\overline{u}_3 - \overline{u}_i) \\ \vdots \\ w'_{iN}(\overline{u}_N - \overline{u}_i) \end{pmatrix}, \tag{22}$$

where

$$L'_{ij} = (w'_{ij}\hat{x}_{ij} w'_{ij}\hat{y}_{ij} w'_{ij}\widehat{x^2_{ij}} w'_{ij}\widehat{xy}_{ij} w'_{ij}\widehat{y^2_{ij}} \cdots) \tag{23}$$

and

$$w'_{ij} = \frac{1}{|\mathbf{x}_j - \mathbf{x}_i|^2} W^{\mathrm{DD}}_{ij}. \tag{24}$$

As data-dependent weights are assigned, the number that are numerically large are counted. If too few control volumes are assigned high data-dependent weights, insufficient smoothly connected data is available to compute the desired number of derivatives. Similarly to the data-independent case, this results in a lowering of the nominal order of accuracy of the reconstruction locally. This loss of accuracy is most likely to occur for control volumes straddling discontinuities; near the intersection of two discontinuities; or near the impingement of a discontinuity on a boundary. Because no nonsmooth data has a significant impact on the reconstruction, however, large overshoots in the reconstruction are not expected. This would not be true if nonsmooth data were included.

3.5. *Comparison with WENO Schemes*

Conceptually, there is a great deal of similarity between WENO schemes and the new DD-L_2-ENO schemes. Both seek to produce a high-order accurate, essentially nonoscillatory reconstruction of a function, eliminating the deleterious effects of using nonsmooth data in reconstructing a function by giving nonsmooth data a weight no larger than the order of the truncation error. In both cases, the weights vary smoothly with changes in the control-volume averaged function, eliminating the ''switching'' behavior found in stencil-searching ENO schemes.

There are, however, several key differences between these two families of schemes:

1. DD-L_2-ENO schemes are inherently multi-dimensional; WENO schemes are designed to be applied dimension by dimension. DD-L_2-ENO schemes are therefore suited for use with unstructured as well as curvilinear structured meshes, while WENO schemes can be used only with structured meshes. This does not preclude the construction of a multidimensional WENO reconstruction scheme capable of reconstructing on unstructured meshes. In outline, one would need to construct for each control volume V_i a set of candidate stencils; reconstruct using each stencil; compute weights for each stencil based on the apparent smoothness of the data; and compute a weighted sum of the stencil reconstructions to obtain the final reconstruction. The most difficult step here is the first: construction of each candidate stencil requires a systematic search for a fixed number of nearby neighbors. Whether these stencils are stored or recomputed for each use is an implementation issue of great consequence for the CPU and memory resources required by such a scheme.

2. WENO schemes can be designed to produce $(2k + 1)$ order accurate reconstruction for smooth data in a single dimension [7]. This is done by choosing weights for each of $k + 1$ $(k + 1)$-point stencils so that successive truncation error terms are annihilated. This possibility is latent in DD-L_2-ENO schemes; given a stencil that contains all the points used in such a high-order WENO reconstruction, an equal number of derivatives could be accurately calculated. However, the emphasis in developing DD-L_2-ENO schemes has been on application to irregular, multidimensional geometries. For these cases, dimension-by-dimension reconstruction fails and, because the number of derivatives grows as k^D, required stencil sizes for such high accuracy grow very rapidly in multiple dimensions. For this reason, DD-L_2-ENO was not designed with such high accuracy in mind.

3. DD-L_2-ENO schemes weigh points individually, while WENO schemes apply weights to stencils. In one dimension, this difference is probably moot; the same points are likely to have high weights either way. In multiple dimensions, the difference between schemes will depend on how multidimensional WENO stencils are chosen. It is probable that some smoothly connected data would be ignored by a multidimensional WENO scheme. Whether this would make a practical difference in the reconstruction is far less clear.

4. DD-L_2-ENO schemes have a built-in mechanism to allow accuracy degradation when insufficient smooth data exists. Specifically, if too little smoothly connected data exists, the degree of the reconstruction is automatically

reduced to a level for which there is sufficient smooth data. WENO schemes, like stencil-searching ENO schemes, work from the premise that there *will be* sufficient smooth data if only it can be found. In cases where function discontinuities are very closely spaced, this assumption fails. WENO schemes can produce poor reconstructions here, while DD-L_2-ENO schemes will produce a low-order accurate reconstruction using only smoothly connected (=relevant) data.

3.6. *Summary*

The data-dependent least-squares approach can be used to produce function reconstructions which satisfy the ENO condition. The least-squares heritage of these DD-L_2-ENO schemes allows them to be applied easily to function reconstruction on unstructured meshes in multiple dimensions. The algorithm can be summarized as follows:

- *Input*. A computational mesh, structured or unstructured. For each control volume, the average value of a function to be reconstructed.
- *Output*. An ENO reconstruction of the function, in the form of a modified Taylor series expansion about each vertex, valid within the control volume surrounding the vertex.
- *Preprocessing*. For each control volume V_i, find a sufficiently large set of nearby control volumes $\{V_j\}_i$ for reconstruction of the desired order. Generally, this requires finding first or second neighbors for each vertex.
- *Preprocessing*. Compute all control volume moments that will be needed in the least-squares problem of Eq. (12).
- For each control volume each time a function is reconstructed:

1. Compute geometric weights and construct the arrays needed for the data-independent least-squares problem of Eq. (12).
2. Solve the least-squares problem using Householder transformations. The solution algorithm should not destroy the original arrays and should return both the solution and the residual of the least-squares problem, along with information about how many derivatives were actually calculable.
3. Using the residual of the least-squares problem, compute a data-dependent weight for each control volume in the stencil and multiply the appropriate row of the original least squares problem by this weight. Keep track of how many high weights there are, as this limits the number of derivatives which can be plausibly calculated.
4. Re-solve the least-squares problem. The result gives the derivative terms to be used in the reconstruction of Eq. (3).

4. FUNCTION RECONSTRUCTION

Because the new DD-L_2-ENO scheme is designed for use on unstructured meshes, results will be compared both to ENO reconstructions and to a standard algorithm for unstructured meshes, least-squares reconstruction with Venkatakrishnan's limiter [2].

4.1. *Reconstruction Accuracy for Smooth Functions*

Figure 1 shows the L_1 error in the reconstruction of a sinusoid on a periodic domain using four reconstruction techniques: data-independent least squares, data-independent least squares with Venkatakrishnan's limiter, RP-ENO, and DD-L_2-ENO. In each case, the nominal order of accuracy of the reconstruction is attained, except for the limited reconstruction, which is only first order because of the reduction of gradients near smooth extrema.

4.2. *Solutions of the Scalar Wave Equation*

Solutions to the scalar wave equation in one dimension were computed using a complex initial condition. The scalar wave equation is

$$\begin{aligned} &u_t + u_x = 0, \quad -1 < x < 1, \\ &u(x,0) = u_0(x) \\ &\text{Periodic BC}, \end{aligned} \tag{25}$$

where u_0 is a function given by Jiang and Shu [7]:

$$u_0(x) = \begin{cases} \dfrac{G(x, z-\delta) + 4G(x,z) + G(x, z+\delta)}{6}, & -0.8 \le x \le -0.6, \\ 1, & -0.4 \le x \le -0.2, \\ 1 - |10(x-0.1)|, & 0 \le x \le 0.2, \\ \dfrac{F(x, a-\delta) + 4F(x,a) + F(x, a+\delta)}{6}, & 0.4 \le x \le 0.6, \\ 0, & \text{otherwise}, \end{cases} \tag{26}$$

with

$$\begin{aligned} G(x,z) &= \exp(-\beta(x-z)^2) \\ F(x,a) &= \sqrt{\max(0, 1-\alpha^2(x-a)^2)} \end{aligned} \qquad \begin{cases} a = 0.5 \\ z = -0.7 \\ \delta = 0.005 \\ \alpha = 10 \\ \beta = \log 2/36\delta^2. \end{cases} \tag{27}$$

Figure 2 shows the result of propagating this function

to $t = 8$ on a mesh with 200 points using fourth-order Runge–Kutta time advance with a CFL number of 0.4. Only third- and fourth-order solution are shown; the second-order solutions are all highly smeared. The third-order DD-L_2-ENO scheme performs nearly identically to the third-order RP-ENO scheme; each is much better than the DI-L_2 result, which contains significant overshoots. For fourth-order nominal accuracy, RP-ENO is slightly better than DD-L_2-ENO for all four profiles.

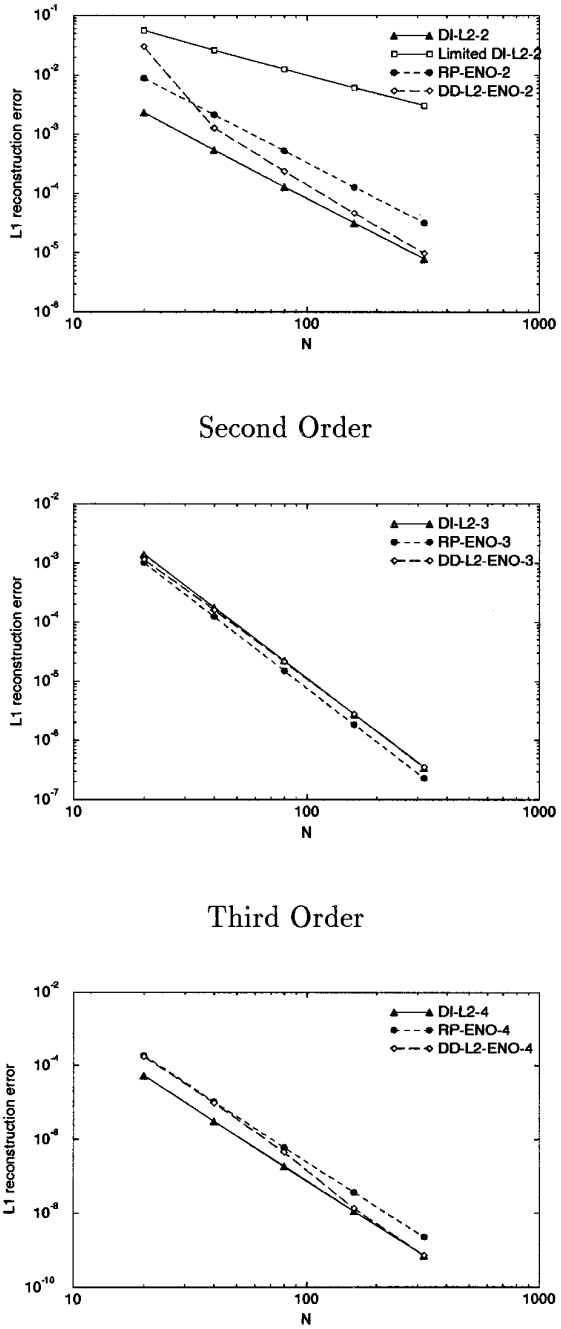

FIG. 1. Reconstruction of a smooth function.

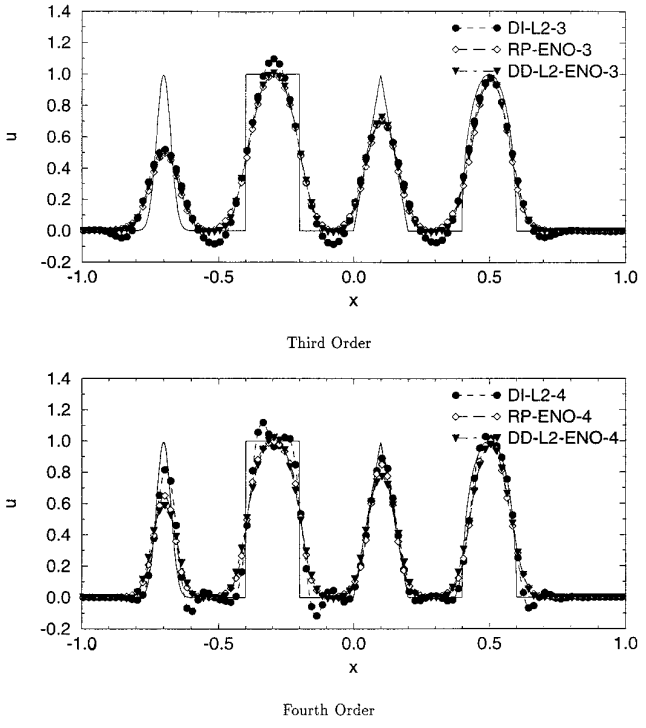

FIG. 2. Linear wave propagation.

4.3. *Nonsmooth Function Reconstruction in Two Dimensions*

The new reconstruction scheme was tested for nonsmooth function reconstruction in two dimensions. The function chosen is that of Abgrall [9][1]

$$u(x,y) = \begin{cases} f(x - \cot\sqrt{(\pi/2)}y), & x \le \cos \pi y/2, \\ f(x + \cot\sqrt{(\pi/2)}y) + \cos(2\pi y), & x > \cos \pi y/2, \end{cases} \tag{28}$$

with

$$f(r) = \begin{cases} -r\sin\left(\dfrac{3\pi}{2}r^2\right), & r \le -\dfrac{1}{3}, \\ |\sin(2\pi r)|, & |r| < \dfrac{1}{3}, \\ 2r - 1 + \dfrac{1}{6}\sin(3\pi r), & r \ge \dfrac{1}{3}. \end{cases} \tag{29}$$

[1] Several typographical errors in the definition of this function in [9] cause a mismatch with the plotted function therein; the function shown here matches the plots in [9].

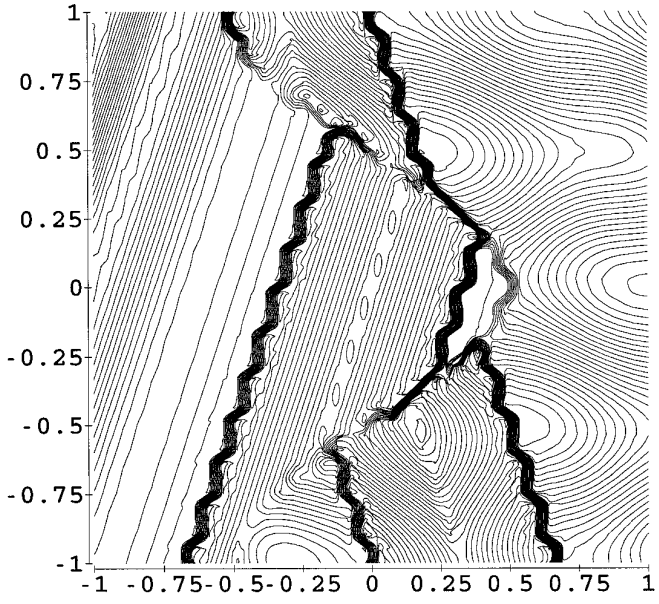

FIG. 3. Contours of the function defined by Eq. (28).

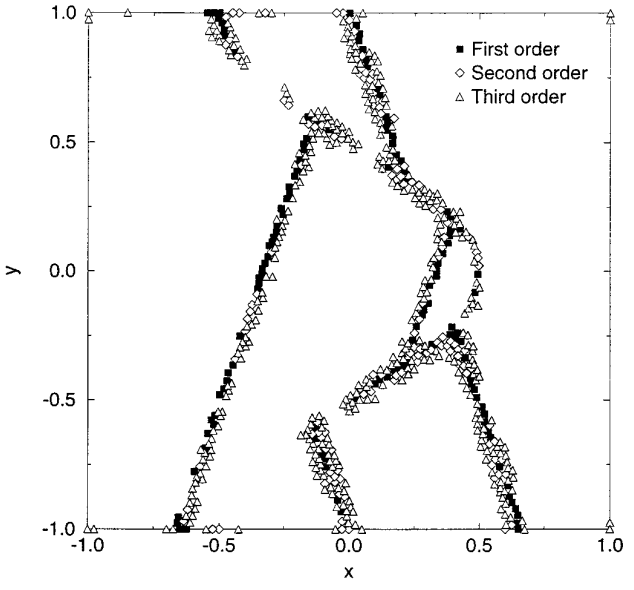

FIG. 5. Control volumes which fail to attain fourth-order accuracy ($k = 3$).

Contour plots of this function are shown in Fig. 3. Because the reconstruction scheme is k-exact, we know that the accuracy of the reconstruction in smooth regions of the function will be of order $k + 1$. Norms of the error in the reconstruction are meaningless in this context, because the difference between the actual function and its reconstruction is guaranteed to be $O(1)$ in control volumes that are crossed by a discontinuity. Instead, for nominal third- and fourth-order accuracy, respectively, Figs. 4 and 5 show the control volumes for which the nominal order of accuracy was not obtained. Traces of the discontinuities can be clearly seen in both figures, with control volumes showing degraded accuracy usually losing only one order (84% for third-order, 59% for fourth). Also, full accuracy is generally obtained on the boundary until the fourth order, for which some control volumes lack enough second neighbors for the reconstruction. No attempt has been made to further extend these stencils into the interior of the mesh to remedy this problem.

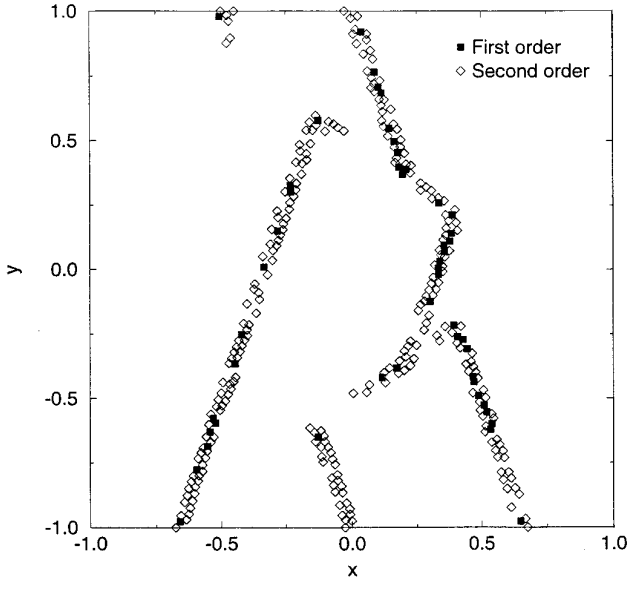

FIG. 4. Control volumes which fail to attain third-order accuracy ($k = 2$).

5. INVISCID FLOW SOLUTIONS

The reconstruction of Section 3 can easily be extended to systems. The approach taken here is to reconstruct all components simultaneously. In this case, the least squares problem of Eq. (12) has as many columns on the right-hand side as there are components in the system. The expression for the residual $\mathscr{R}$ is extended to be

$$\mathscr{R} = \sqrt{(1/C)\sum_{c=1}^{C}\sum_{l=m+1}^{n} r_{l,c}^2}, \tag{30}$$

where C is the number of columns. In the present work, primitive variables $(\rho\ u\ P)^{\mathrm{T}}$ are used for reconstruction throughout, and the density is chosen to compute the smoothness indicator. As in the scalar case, the least-squares problem is modified by multiplication of each row by the data-dependent weight for that control volume, and a second least-squares problem is solved.

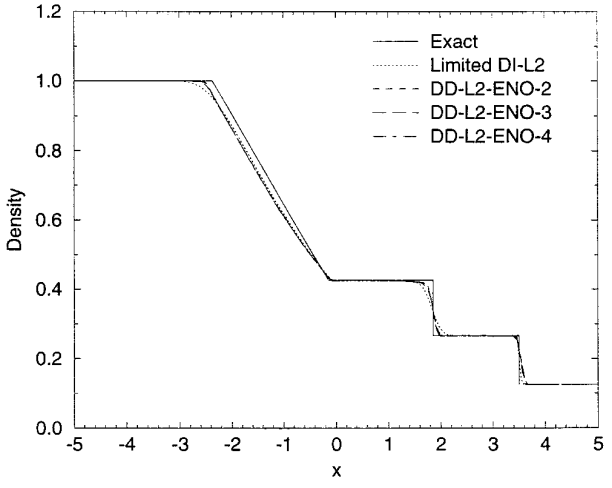

FIG. 6. Density plots for Sod's shock tube problem.

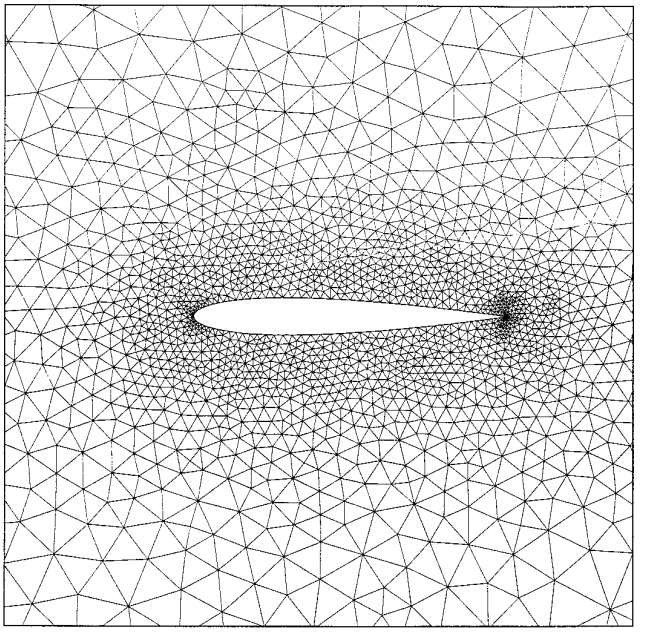

FIG. 7. Mesh for high α case; 3323 vertices.

5.1. *Sod's Problem*

The first result presented is the solution of Sod's shock tube problem in one dimension. The initial conditions are

$$(\rho\, u\, P)(x,0) = \begin{cases} (1\ 0\ 1), & x < 0, \\ (\frac{1}{8}\ 0\ \frac{1}{10}), & x > 0. \end{cases} \tag{31}$$

Fourth-order Runge–Kutta time advance was used with a CFL number of 0.6 on a 400-point mesh. Note that reconstruction for this problem used primitive variables, not characteristic variables. Density at $t = 2$ is shown in Fig. 6. The data-dependent schemes provide better resolution near the contact discontinuity and the ends of the expansion fan while keeping overshoots acceptably small. The contact discontinuity becomes progressively sharper with increasing order of accuracy and accuracy near the head of the expansion improves similarly.

5.2. *Two-Dimensional Inviscid Airfoil Problems*

To demonstrate solution accuracy for two-dimensional aerodynamics problems, two inviscid flow results will be shown. For both cases, the flow solver is a multigrid scheme using three coarse meshes. Multistage time advance is used, along with local preconditioning [12, 13]. The CFL number is 0.8, and the multistage coefficients are {0.5321, 1.3711, 2.7744}.

The first test case is a high angle of attack flow around a NACA 0012 airfoil, at $M = 0.302$ and $\alpha = 9.86°$. Figure 7 shows the fine mesh used for this case, which contains 3323 vertices. The solution was computed by using unlimited DI-L_2, limited DI-L_2 (Venkatakrishnan's limiter [2]), and unlimited second-order DD-L_2-ENO. The solutions are virtually identical except near the suction peak on the upper surface. A detail of the surface pressure coefficient in this region is shown in Fig. 8; the figure also includes a solution from INS2D to which the Karman–Tsien pressure correction has been applied. The two unlimited reconstruction schemes give identical results to plotting accuracy; the limited scheme comes slightly closer to capturing the suction peak. The limited resolution near the leading edge prevents any of the three solutions from matching the suction peak computed by INS2D on a fine mesh.

AGARD test case 1 [14] was used to test the new scheme for flows with shock waves. This case computes flow around

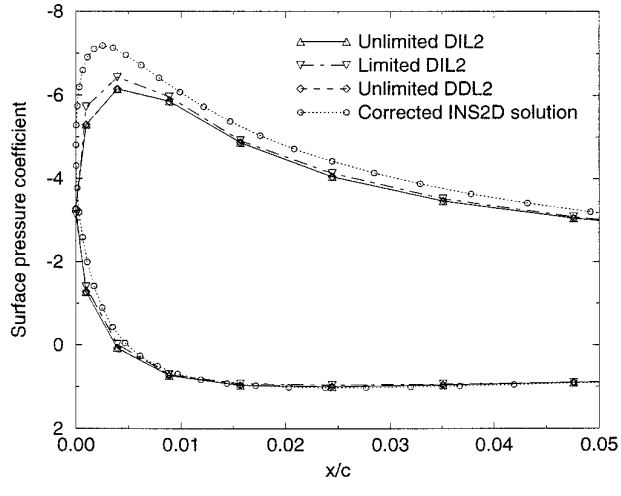

FIG. 8. Surface C_p near suction peak.

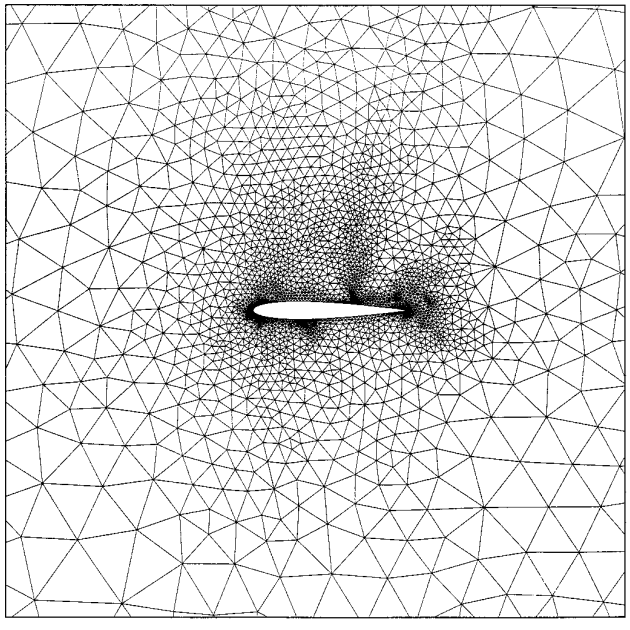

FIG. 9. Mesh for AGARD Test Case 1; 4156 vertices.

a NACA 0012 airfoil at a Mach number of 0.8 and an angle of attack of 1.25°. A mesh with 4156 vertices was used (see Fig. 9).

The solution was computed by using both limited DI-L_2 reconstruction and second-order DD-L_2-ENO reconstruction. The surface pressure coefficients for these two solutions and for the accepted AGARD solution [14] are given in Fig. 10. An inset shows a close-up of the upper-surface shock, which is shifted by one mesh vertex between the two solutions. The quality of the solutions using limited DI-L_2 reconstruction and unlimited DD-L_2-ENO reconstruction are comparable.

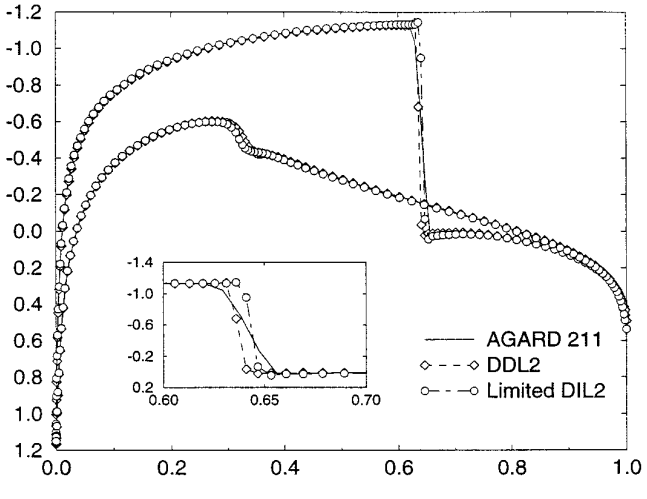

FIG. 10. Surface pressure coefficient for AGARD Test Case 1.

6. CONCLUSIONS

A new method for function reconstruction has been described that combines the best features of least-squares and ENO reconstructions. This new scheme, DD-L_2-ENO, uses a data-dependent weighting in least-squares reconstruction to satisfy the ENO condition of Liu, Osher, and Chan [6]. Like other ENO schemes, DD-L_2-ENO is uniformly accurate, even in the presence of discontinuities, and allows only asymptotically small overshoots.

Because DD-L_2-ENO is a least-squares reconstruction procedure, existing efficient algorithms for least-squares reconstruction can be easily modified for DD-L_2-ENO. An algorithm for computing DD-L_2-ENO reconstructions of arbitrary order on unstructured meshes is given. The data-dependent weights used in the scheme vary continuously with the data and consequently good convergence behavior is anticipated for steady-state calculations. The stencil for DD-L_2-ENO is larger than that required by conventional ENO schemes, but no larger than required by k-exact least-squares reconstructions of the same order of accuracy.

The asymptotic behavior of the scheme in reconstructing smooth and piecewise smooth functions has been demonstrated. DD-L_2-ENO produces uniformly high-order accurate reconstructions, even in the presence of discontinuities. The new scheme behaves comparably to RP-ENO in solving the scalar wave equation in one dimension.

A feature of the new scheme is its ability to detect and control situations where insufficient smooth data exists for the desired order of reconstruction. In such cases, the scheme automatically determines the amount of smooth data present and computes a reconstruction of appropriately reduced accuracy. This capability was demonstrated by reconstructing a nonsmooth function; control volumes for which insufficient smooth data existed were shown to have a lower-order reconstruction computed instead.

Extension of the reconstruction scheme to systems was discussed. As examples of the behavior of such reconstructions, solutions were shown for the Sod shock tube problem in one dimension and for two aerodynamic problems in two dimensions. These early two-dimensional results are very encouraging. In all cases, solution accuracy was comparable to existing schemes suitable for unstructured meshes and overshoots in the solution were of acceptable magnitude.

ACKNOWLEDGMENTS

The author thanks Tim Barth for numerous helpful discussions on k-exact reconstruction, Michael Aftosmis for reading and commenting on an early draft of this paper, and the reviewers for helpful comments which pointed out several weaknesses in the exposition. This work was supported in part by the Mathematical, Information, and Computational Sciences Division subprogram of the Office of Computational and Technology Research, U.S. Department of Energy, under Contract W-31-109-

Eng-38; and in part by the National Research Council while the author was a Research Associate at NASA Ames Research Center.

REFERENCES

1. T. J. Barth and P. O. Frederickson, AIAA Paper 90-0013, Jan. 1990 (unpublished).
2. V. Venkatakrishnan, AIAA Paper 93-0880, Jan. 1993 (unpublished).
3. A. Harten and S. Osher, Uniformly high-order accurate nonoscillatory schemes, *SIAM J. Numer. Anal.* **24,** 279 (1987).
4. A. Harten, S. Osher, B. Engquist, and S. R. Chakravarthy, Some results on uniformly high-order accurate essentially non-oscillatory schemes, *Appl. Numer. Math.* **2,** 347 (1986).
5. A. Harten, B. Enquist, S. Osher, and S. R. Chakravarthy, Uniformly high order accurate essentially non-oscillatory schemes, III, *J. Comput. Phys.* **71,** 231 (1987).
6. X.-D. Liu, S. Osher, and T. Chan, Weighted essentially non-oscillatory schemes, *J. Comput. Phys.* **115,** 200 (1994).
7. G.-S. Jiang and C.-W. Shu, Efficient implementation of weighted ENO schemes, *J. Comput. Phys.* **126,** 202 (1996).
8. L. J. Durlofsky, B. Enquist, and S. Osher, Triangle based adaptive stencils for the solution of hyperbolic conservation laws, *J. Comput. Phys.* 98, 64 (1992).
9. R. Abgrall, On essentially non-oscillatory schemes on unstructured meshes: Analysis and implementation, *J. Comput. Phys.* **114**(1), 45 (1994).
10. T. J. Barth, AIAA Paper 93-0668, Jan. 1993 (unpublished).
11. G. H. Golub and C. F. van Loan, *Matrix Computations* (Johns Hopkins Univ. Press, Baltimore, MD, 1983).
12. C. F. Ollivier-Gooch, Multigrid acceleration of an upwind Euler solver on unstructured meshes, *AIAA J.* 33, 1822 (1995).
13. C. F. Ollivier-Gooch, ''Towards Problem-Independent Multigrid Convergence Rates for Unstructured Mesh Methods I: Inviscid and Laminar Viscous Flows,'' in *Proceedings, Sixth International Symposium on Computational Fluid Dynamics, Japan Society of Computational Fluid Dynamics, University of California at Davis, Sept. 1995.*
14. AGARD Fluid Dynamics Panel, *Test Cases for Inviscid Flow Field Methods* (AGARD, May 1985); AGARD Advisory Report AR-211.